Optical Materials 84 (2018) 8–15

Contents lists available at ScienceDirect

Optical Materials

journal homepage: www.elsevier.com/locate/optmat

New ruthenium(II) bipyridine complex bearing 2-aminophenylbenzimidazole: Synthesis, spectral characterization and optical properties

Shadia A. Elsayed[a], Eman A. Gaml[b,*], M.A. Nasher[b,c]

[a] Department of Chemistry, Faculty of Science, Damietta University, New Damietta, 34517, Egypt
[b] Department of Physics, Faculty of Science, Damietta University, New Damietta, 34517, Egypt
[c] Department of Physics, Faculty of Science, Sadah University, Sadah, Yemen

ARTICLE INFO

Keywords:
Ru(II)bipyridine
Spectra
XRD
Optical properties
Thin films

ABSTRACT

The new bipyridine-based ruthenium(II) complex $[Ru(bpy)_2(Hapbim)]^{2+}$ (bpy being 2,2′-bipyridine, and Hapbim is 2-aminophenylbenzimidazole) was synthesized and characterized. On the basis of elemental analysis, spectroscopic techniques (FTIR, ^{1}H NMR, UV-Visible), magnetic, conductivity and thermal analysis measurements, it was found that the Hapbim ligand coordinates to Ru(II) kernel in a neutral bidentate fashion through cyclic azomethine N of benzimidazole moiety along with the terminal nitrogen of the amino group forming six-membered chelate ring. Thin films of the Ru(II)-complex were prepared using thermal evaporation technique. The thin film structure was characterized using FTIR and X-Ray diffraction techniques. FTIR analysis revealed that the complex is chemically stable under both thermal evaporation and thermal annealing. The optical properties were studied by spectrophotometric measurements. The optical constants of the complex were calculated and it is found to have 1.5 eV band gap. Also, the effect of thermal annealing on the optical properties of the complex is studied. Annealing of the complex thin films increased the values of the dispersion parameters and decreased the value of the band gap.

1. Introduction

Transition metal complexes of nitrogen donor chelating agents are well known for their various applications in many research fields including biology [1], catalysis, solar power conversion and its storage [2–4]. In particular, ruthenium complexes bearing polypridyl ligands are of a considerable interest due to their photo-physical/chemical, electrochemical properties and high photochemical stability [5]. These complexes play important roles in several research areas including light emitting diodes [6], electroluminescent devices, dye sensitized solar cells [7,8], and solar energy conversion [9].

Ruthenium(II) containing 2,2′-bipyridine (bpy) have interesting properties including strong absorption of light in visible region due to metal-to-ligands charge transfer (MLCT), also their excited states have relatively long lifetime because of the forbidden transition from triplet excited state to singlet ground state [10–12]. The replacement of bpy by heterocyclic compounds containing N-donors has gained noticeable attention in recent time, due to the changes in their photochemical and photophysical properties occurred by incorporating these units [13]. The optical properties of the ruthenium complexes demonstrate significant device performance when prepared as thin films [14,15]. In addition to ruthenium(II) complexes, thin films of cobalt(II) and Mn(II) complexes containing benzimidazole moiety were prepared and structurally characterized, it was proven that annealing of thin films of these metal complexes improved their surface homogeneity as well as enhancement of their optical transmittance [16,17]. Manjunatha et al. [18] have reported the preparation of thin films from $[Ru\text{-salophen}]^{2+}$ complex (salophen = N, N' -disalicylidene-1,2-ethylendiimine) using a spin coating technique. The obtained data revealed that the complex exhibited a relatively large non-linear optical properties (NLO) along with optical switching behavior which enables it to be a promising material for fabricating optoelectric devices.

In this work, we report the synthesis of new ruthenium(II) bipyridine complex of 2(2′-aminophenyl)-1H-benzimidazole (2-aminophenylbenzimidazole) $[Ru(bpy)_2(Hapbim)]^{2+}$. Its structure was elucidated by means of spectroscopy (FTIR, ^{1}H NMR, UV-visible), thermal, magnetic, and molar conductivity measurements. Thin films of this complex were prepared and characterized along with investigating the effect of annealing on its optical properties. The molecular structures of the ligand and complex are shown in Figs. 1 and 2, respectively.

* Corresponding author.
E-mail address: emangamlph@gmail.com (E.A. Gaml).

https://doi.org/10.1016/j.optmat.2018.06.052
Received 24 April 2018; Received in revised form 20 June 2018; Accepted 21 June 2018

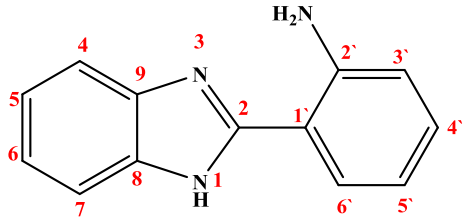

Fig. 1. Structure of structure of 2(2′-aminophenyl)-1H-benzimidazole with atom numbering scheme.

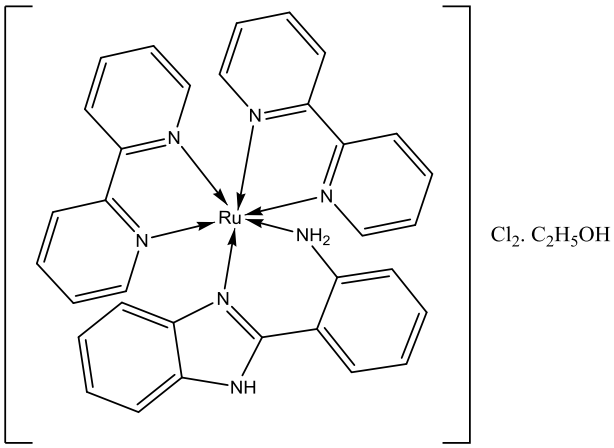

Fig. 2. Structure of $[Ru(bpy)_2(Hapbim)]Cl_2.C_2H_5OH$ complex.

2. Experimental

2.1. Materials and methods

2-aminophenylbenzimidazole and 2,2′-bipyridine were purchased from Alfa Aesar. *Cis*-$[Ru(bpy)_2Cl_2].2H_2O$ was prepared as reported elsewhere [19]. All solvents and reagents were used as received.

2.2. Instrumentation

Infrared spectroscopy was performed on JASCO 4100 FTIR spectrometer (4000 - 400 cm^{-1}) on KBr disc. ^1H NMR spectra were recorded in DMSO-d_6 on Bruker 400 MHz Electronic spectra (200–900 nm) were measured in ethanol using JASCO V- 630 spectrometer. Elemental analyses (C, H, N) were carried out at microanalytical unit at Cairo university. Magnetic susceptibility value of the complex was obtained using Johnson Matthey magnetic susceptibility balance. Molar conductivity of the complex (in CH_2Cl_2) was measured on YSI Model 32 Conductivity Bridge at room temperature. Thermal analysis data were collected in the temperature range 20–800 °C under nitrogen atmosphere 15.00 ml/min using Shimadzu TGA-50 instrument at a heating rate of 20 °C/min. Thin films of the powder phase of Ru-complex were prepared by thermal evaporation technique using Edwards (E306 A) coating unit. The powder of the complex was sublimated from quartz crucible into optically flat quartz substrates. The pressure during evaporation process was 10^{-5} Torr and the evaporation rate was maintained at 0.5 nm/s. The film thickness was measured using quartz crystal thickness monitor (Model TM-350 MAXTEK, Inc. USA) attached to the coating system. Thin films of the Ru(II)-complex were annealed at 423 K for 30 min. The X-Ray diffraction, XRD, measurements for the as synthetized powder, as deposited, and annealed thin films were carried out using Philips X-ray diffraction system, model X'Pert MPD. The operating voltage and current for the X-ray tube were 50 kV and 40 mA, respectively. The spectral data of transmittance and reflectance at nearly normal incidence were collected using spectrophotometric measurements by using double beam spectrophotometer JASCO model (V-570-UV-Vis.-NIR) in the wavelength range 200–2500 nm.

2.3. Optical constants calculation

To calculate the values of the refractive index (n), absorption coefficient (α) and the absorption index (k), we substitute the calculated values of the transmittance, T and reflection R in equation (1–3) [20]:

$$n = \left(\frac{1+R}{1-R}\right) + \left(\frac{4R}{(1-R)^2} - k^2\right)^{1/2} \quad (1)$$

$$\alpha = \frac{1}{d} Ln\left(\frac{(1-R)^2}{2T} + \sqrt{\frac{(1-R)^4}{4T^2} + R^2}\right) \quad (2)$$

$$k = \frac{\alpha\lambda}{4\pi} \quad (3)$$

2.4. Synthesis

To an ethanolic solution of 2-aminophenylbenzimidazole (0.5 mmol, 0.105 g, 25 mL), *cis*-$[Ru(bpy)_2Cl_2].2H_2O$ (0.5 mmol, 0.26 g) was added. The reaction mixture was refluxed for 12 h during which the purple color of the solution turned dark red. The solution was then concentrated to one-third of its volume. The reddish brown precipitate was formed by adding an excess amount of diethyl ether. The product was collected by filtration through a sintered glass gooch, washed with ether, then dried in *vacuo*. Yield 0.23 g (67%), mp > 200 °C. Diamagnetic (μ_{eff} = 0 B M), molar conductance (10^{-3} M in CH_2Cl_2, Λ_M) = 180 Ω^{-1} cm^2 mol^{-1}. Elemental analysis (%) for $C_{35}H_{33}Cl_2N_7ORu$ (Mw = 739.67), Calcd (Found): C, 56.83 (56.78); H, 4.50 (4.10); N, 13.26 (13.0). FTIR (KBr, cm^{-1}): ν(NH) 3330, $\nu(NH_2)$ 3130, ν(C=N), 1597, ν(C=C) 1495–1520, ν(CH), 2998–3030, ν(Ru-N) 422. ^1H NMR (400 mHz, DMSO-d_6, δ ppm): 14.70 (1H, s, N(1)H), 7.43 (N(2′)H_2, s, 2H), 6.89 (1H, d, H(3′), J = 8.10 Hz); 7.89 (1H, d, (H(6′)), J = 7.6 Hz); 8.23 (1H, d, H(7), J = 6.6 Hz); 7.84 (1H, d, H(4), J = 6.5 Hz); 7.30–7.73(4H, m, H(4′, 5′, 5,6)); 8.8–9.05 (4H, d, H(3,3′), J = 7.6, 8.0, bpy); 8.01–8.1 (4H, m, H(4,4′), bpy); 7.61–7.66 (4H, m, H(5,5′), bpy); 8.70–8.78 (4H, d, (H6,6′), J = 8.0, 8.0 Hz, bpy); 4.38 (1H, s, $CH_3CH_2O\underline{H}$), 3.44 (2H, q, ($CH_3C\underline{H}_2OH$, J = 6.8 Hz), 1.06 (3H, t, $C\underline{H}_3CH_2OH$, J = 7.2 Hz). UV-Vis (EtOH, 1 × 10^{-5} M): λ_{max} (nm) (ε, L.mol^{-1}. cm^{-1}): 294 (78000), 356 (14700) and 499 (8500).

3. Results and discussion

3.1. Synthesis

The complex $[Ru(bpy)_2(Hapbim)]Cl_2.C_2H_5OH$ was prepared by the reaction of *cis*-$[Ru(bpy)_2Cl_2].2H_2O$ with 2-aminophenyl benzimidazole (Hapbim) in ethanol in 1:1 M ratio under reflux condition. The complex was powder-like, readily soluble in water and common organic solvents such as methanol, ethanol, CH_2Cl_2, DMF and DMSO. The molar conductance value of the complex was 180 Ω^{-1} cm^2 mol^{-1} to indicate that the complex is ionic in nature with two chlorides as counter ions (2:1).

3.2. FTIR spectra

The FTIR spectrum of the of 2-aminophenyl benzimidazole ligand (Fig. 3 a) shows two medium bands at 3383 and 3140 cm^{-1} assigned to the stretching vibrations of ν(NH) of NH_2 and ν(NH) of benzimidazole, respectively [21–23]. The spectrum of the complex (Fig. 3 b), reveals the shift of those bands to 3030–3383 cm^{-1} to lower frequency suggesting the participation of NH_2 nitrogen in the coordination to Ru(II) center. The sharp band observed at 1608 cm^{-1} assigned to ν(C=N) in the ligands is shifted in the complex to a lower frequency by

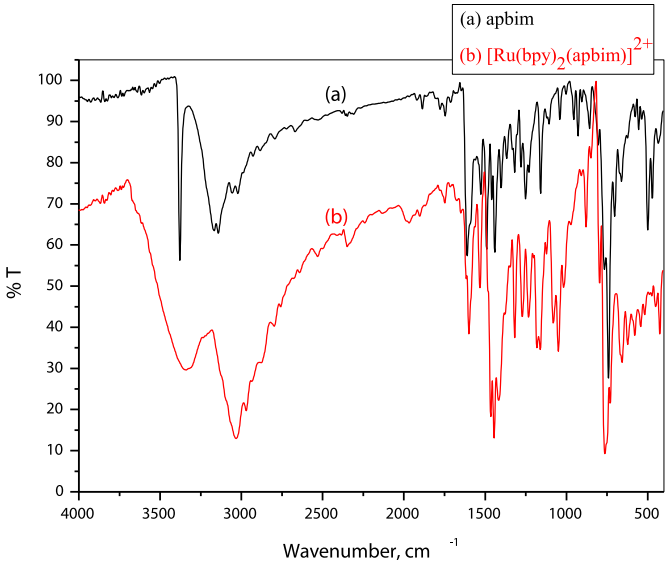

Fig. 3. FTIR spectra (a) ligand and (b) complex in powder.

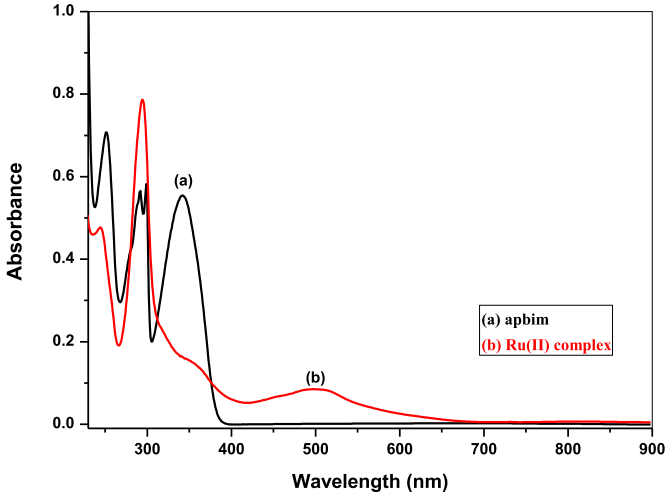

Fig. 5. UV-Vis absorption spectra of the ligand and $[Ru(bpy)_2(apbim)]^{2+}$ complex in ethanol (1×10^{-5} M).

$\sim 12\,cm^{-1}$, confirming the coordination of cyclic azomethine nitrogen of benzimidazole unit (N(3)). The above mentioned observations indicate that Hapbim ligand coordinated to ruthenium in a bidentate neutral form (Fig. 2). The other bands detected for the free ligand and complex around 2998–3030 cm^{-1} and 1495–1520 cm^{-1} regions are due to ν(CH) and ν(C=C) vibrations, respectively. The new band appeared at 422 cm^{-1} in the complex spectrum is assigned to ν(Ru-N) [24]. FTIR analysis of the as deposited and annealed at 423 K thin films were performed and revealed that the complex has almost no changes in band positions. This confirms the thermal stability of the complex powder under thermal evaporation technique. It also proves that the thin film of the complex is thermally stable after annealing process.

3.31H NMR spectra

The structure of the free ligand with its atom numbering Scheme is presented in Fig. 1. The ^{1}H NMR spectrum of the ligand and Ru(II)-complex is shown in Fig. 4a and b. The ^{1}H NMR spectrum of the ligand (Hapbim) exhibits two singlets at δ12.66 and 7.26 ppm due to NH and NH_2 groups, respectively. It also shows four doublets at δ 6.83 (J = 6.8 Hz), 7.51(J = 6.0 Hz), 7.65(J = 6.0 Hz) and 7.84 (J = 6.4 Hz) assigned to H(3′), H(6′), H(7) and H(4), respectively. The doublet of doublets obtained at δ 6.66 (J = 6.0, 6.0 Hz) and 7.16 (J = 6.4, 6.0 Hz) are attributed to H(5′) and H(4′), respectively, while H(5, 6) appeared

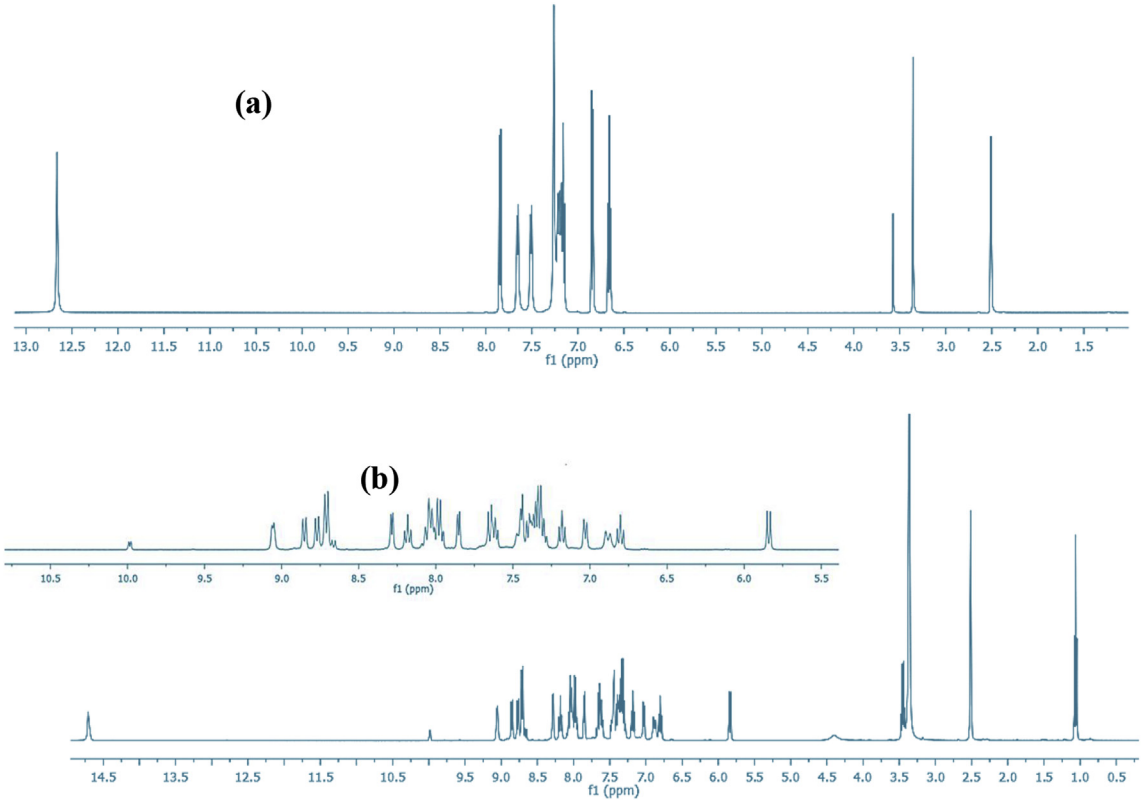

Fig. 4. ^{1}H NMR spectra of (a) ligand and (b) complex.

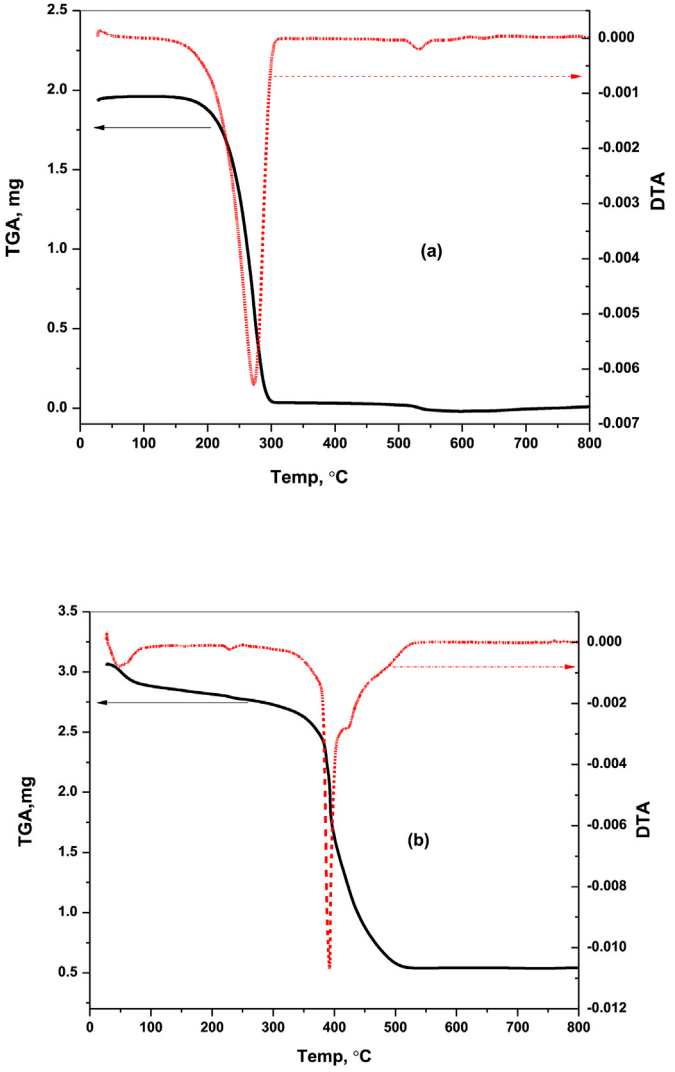

Fig. 6. TGA/DTA thermograph of (a) Hapbim ligand and (b) Ru(II)-complex.

as multiplet at 7.18–7.23 ppm region due to the different environment of protons [22,25–27]. In ^{1}H NMR spectrum of the complex, the resonance arising from N(1)H and N(2)H_2 are shifted downfield to δ 14.7 and 7.43 ppm, respectively due to coordination of NH_2 nitrogen. The new sixteen resonance peaks in the region from 5.83 to 9.06 ppm are assigned to the two 2,2′-bipyridine units [28,29]. At low field resonances, the triplet at 1.06, quartet at 3.44 and singlet at 4.38 ppm are attributed to the protons of ethanol molecule, CH_3, CH_2 and OH, respectively.

3.4. UV-visible spectra measurements

The absorption spectra of Hapbim ligand and its complex were recorded in ethanol in the wavelength range 200–900 nm. The absorption spectra of both the ligand and the complex are shown in Fig. 5. The UV-Vis spectrum of Hapbim shows λ_{max} at 252 nm (ε = 70500 L mol^{-1} cm^{-1}), 291 nm (ε = 56200 L mol^{-1} cm^{-1}) and 341 nm (ε = 55200 L mol^{-1} cm^{-1}) which are attributed to π-π* and n-π* transitions [21]. The UV-Vis spectrum of the diamagnetic ruthenium complex (μ_{eff} = 0 B M) shows its λ_{max} at 294 nm (ε = 78400 L mol^{-1} cm^{-1}) and 356 nm (ε = 14700 L mol^{-1} cm^{-1}) due to the intra-ligand transitions, while the broad band observed at 499 nm (ε = 8500 L mol^{-1} cm^{-1}) may arise from lower energy MLCT (Ru)d → π*(L)/π*(bpy) transition which is lower than 452 nm observed for the unsubstituted $[Ru(bpy)_3]^{2+}$ [30,31]. This observation gives an evidence for the complex formation.

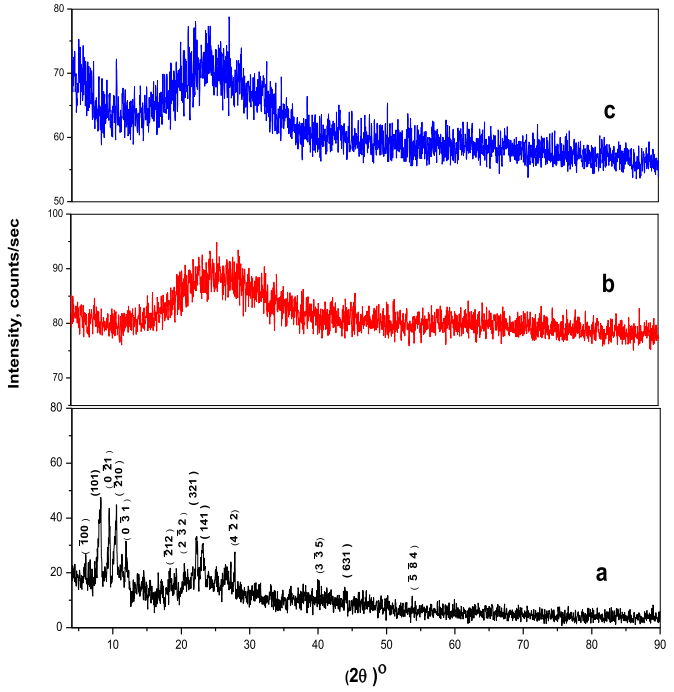

Fig. 7. XRD pattern of the complex in (a) powder form, (b) As deposited thin film and (c) annealed at 423 K Ru(II)-complex thin films.

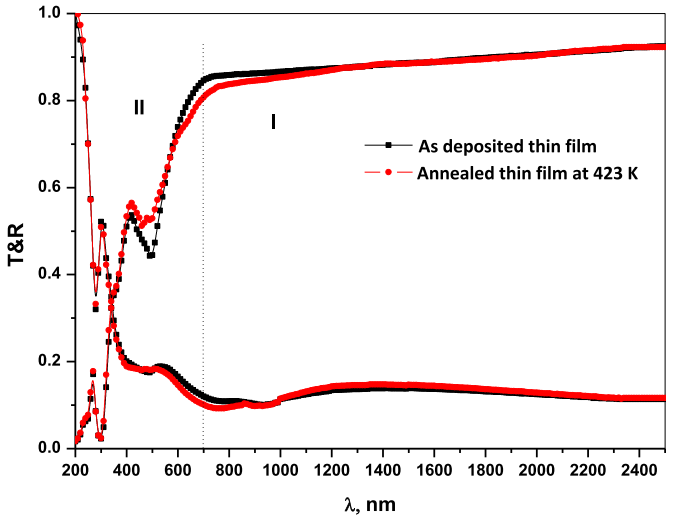

Fig. 8. Spectral behaviors of the Transmittance T, and Reflection R for the As deposited and annealed thin films.

3.5. Thermal analysis

The thermogravimetric analysis (TGA) was carried out to investigate the thermal stability of the ligand and its complex. Their TG/DTA diagrams are shown in Fig. 6a and (b). In TGA/DTA curves of Hapbim ligand (Fig. 6a), the initial degradation starts at ~215 °C and the decomposition occurs in one step process in the temperature range 215–300 °C (endothermic at 275 °C), such decomposition has taken place through the break of N-C bond [32,33]. The TGA/DTA diagrams of the complex (Fig. 6b) show two endothermic decomposition steps; the first step is located in the region 25–100 °C due to the elimination of C_2H_5OH molecule (Found 6.2, Calcd. 6.4%), then up to 300 °C, the complex shows thermal stability. The second step is observed at 300 °C (endothermic at 395 °C) with a total mass loss coincides to weight loss of Cl_2 and 2bpy species followed by degradation of Hapbim ligand

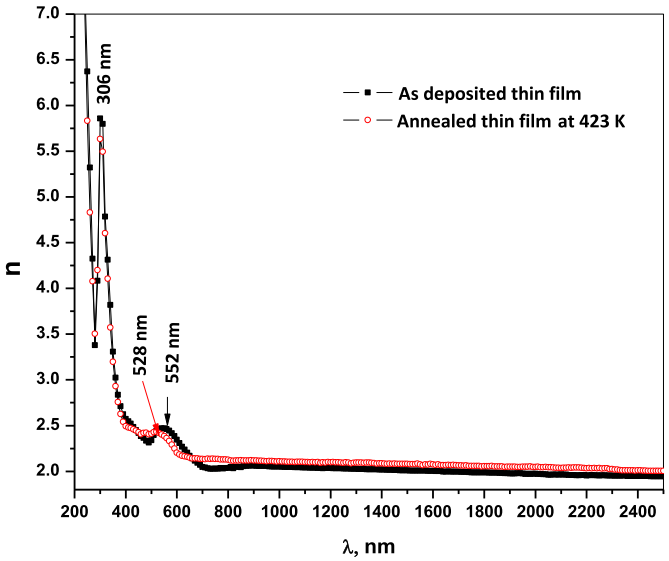

Fig. 9. Effect of annealing on the spectral behavior of the refractive index.

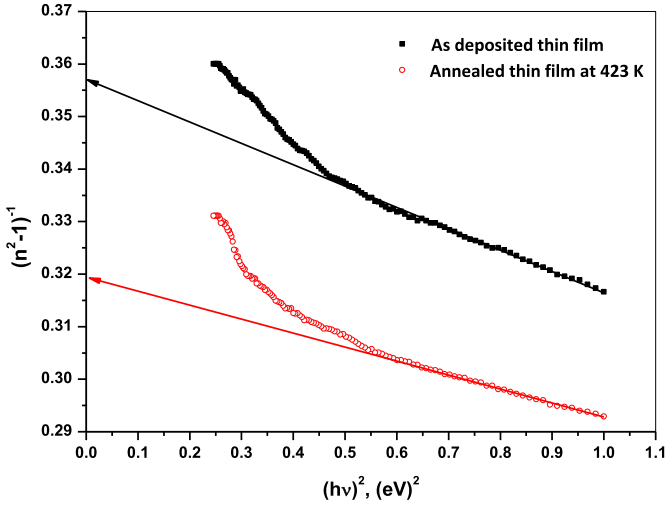

Fig. 10. $(n^2 - 1)^{-1}$ versus $(h\nu)^2$ for the as deposited and annealed Ru-complex thin films.

Table 1
Dispersion parameters for As deposited and annealed at 423 K of Ru-complex thin films.

Film conditions	ε_L	ε_∞	N/m* (g^{-1} cm^{-3})	E_o	E_d
As deposited	5.08	4.02	9.80×10^{43}	2.11	6.38
Annealed at 423 K	5.48	4.20	1.17×10^{44}	2.01	6.44

(Found 75.0, Calcd. 75.9%) [34]. Based on thermal analysis of the ligand and its Ru(II)-complex, it is observed that the complex is more stable than the ligand.

3.6. X-ray diffraction analysis (XRD)

The XRD patterns of the synthesized Ru(II)-complex in powder form, as deposited and annealed thin films are shown in Fig. 7. The XRD pattern for the powder form of the complex shows many diffraction peaks of different intensities indicating its polycrystalline structure [20]. The XRD pattern of the complex in powder form was analyzed using FULLPROOF program [35]. Analysis of the XRD pattern revealed that it has triclinic crystal system with space group p1 and lattice

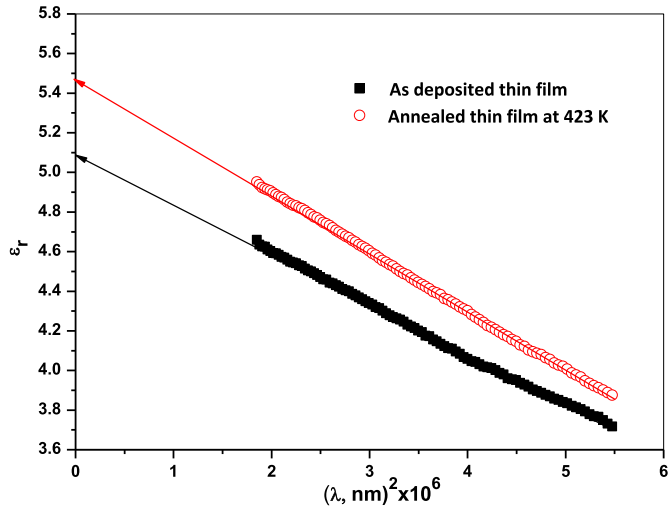

Fig. 11. Versus λ^2 for as deposited and annealed Ru-complex thin films.

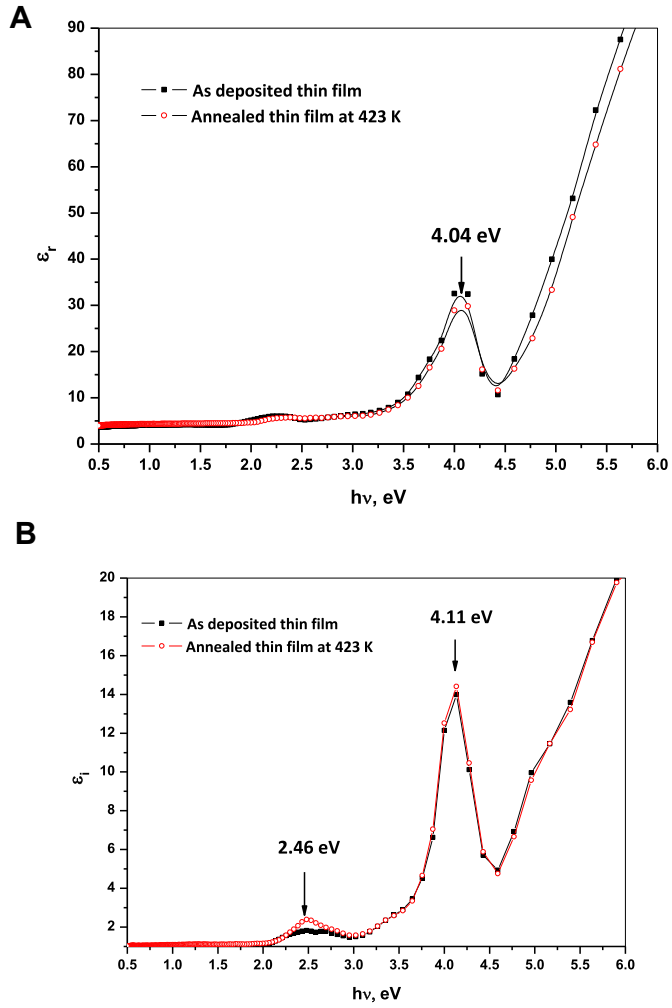

Fig. 12. Effect of annealing on a) ε_r, and b) ε_i of Ru-complex thin films.

parameters a = 15.810 Å, b = 19.64 Å, c = 12.91 Å, α = 100 °, β = 90 °, γ = 100°. It is also observed from Fig. 7 that the XRD patterns of the as deposited and annealed films exhibit a hump at 2Θ *of* 25° which indicate that thin films of the complex have amorphous structure.

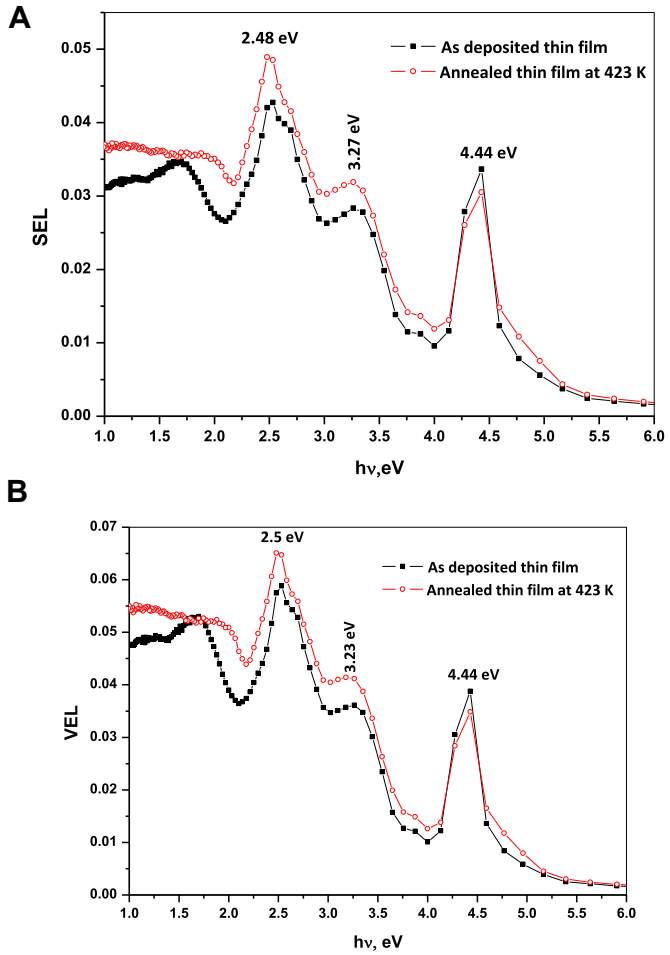

Fig. 13. Effect of annealing on a) *SELF*, and b) *VELF* of Ru-complex thin films.

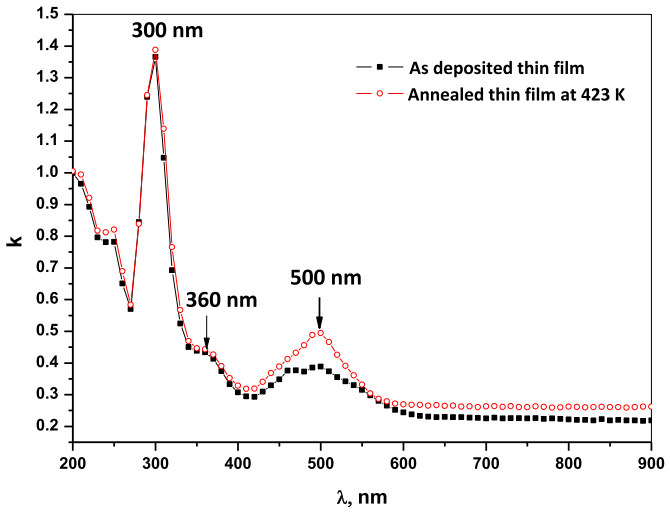

Fig. 14. Spectral behavior of the absorption index, k for the as deposited and annealed at 423 thin films.

3.7. Optical properties of as deposited and annealed thin films of Ru(II)-complex

3.7.1. Spectral behavior of the transmittance, T, and reflectance, R

The spectral behaviors of T and R for as deposited and annealed Ru (II)-complex thin films are depicted in Fig. 8. It is noticed that there are two regions in the spectra separated by sharp absorption edge. Region I

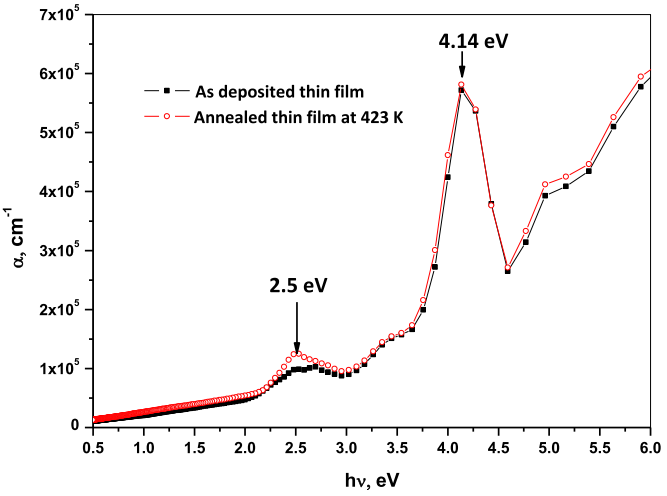

Fig. 15. Effect of annealing on the absorption coefficient, α, for Ru-complex thin films.

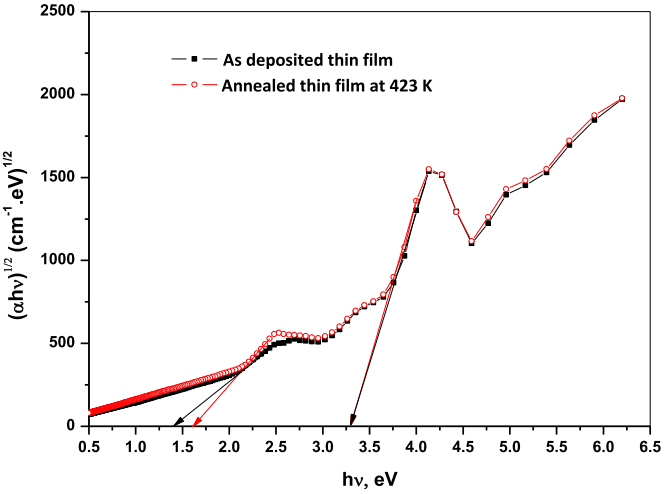

Fig. 16. $(\alpha h\nu)^{1/2}$ versus $h\nu$ for as deposited and annealed Ru-complex thin films.

Table 2
Energy gaps for As deposited and annealed at 423 K Ru-complex thin films.

Optical energy gap, eV	Onset energy gap, eV	Film conditions
3.31	1.49	As deposited
3.38	1.38	Annealed at 423 K

at $\lambda \geq 700\ nm$; where R + T ≈ 1 and no light is absorbed or scattered indicating that the film is homogenous [36]. Region II at $\lambda \leq 700\ nm$; where R + T < 1, this is called the absorption region [37].

3.7.2. Dispersion analysis

The spectral distribution of the refractive index (n) for the as deposited and annealed Ru(II)-complex thin films are illustrated in Fig. 9. It is observed that the normal dispersion behavior is dominant for the wavelengths of $\lambda \geq 700\ nm$ and the single oscillator model can be applied to that region. However at $\lambda \leq 700\ nm$, anomalous dispersion behavior of the refractive index is dominant as revealed by the two dispersion peaks at 306 and 552 nm. After annealing of the film, the dispersion peak at 552 nm is shifted to 528 nm and the refractive index decreases by annealing in the anomalous dispersion region, but increases in the normal dispersion region. The spectral dependence of the refractive index in the normal dispersion region can be analyzed in

terms of the single oscillator model proposed by Wemple and Didomenico [38]. The refractive index is related to the incident photon energy ($h\nu$) by equation (4):

$$(n^2 - 1)^{-1} = \frac{E_d E_o}{E_o^2 - (h\nu)^2} \quad (4)$$

where E_d is the dispersion energy and E_o is the oscillator energy. To calculate the values of E_d and E_o; plots of $(n^2 - 1)^{-1}$ versus $(h\nu)^2$ for as deposited and annealed Ru(II)-complex thin films are shown in Fig. 10. The calculated values of E_d and E_o are listed in Table 1.

The complex dielectric function, ε^* describes the optical response of the medium at all photon energies. The real part of the dielectric constant and the imaginary part show how much a dielectric material absorbs energy from an electric field due to the dipole motion. The real part, ε_r, and the imaginary part, ε_i, of the complex dielectric constant were calculated by equation [20]:

$$\varepsilon_r = n^2 - k^2 = \varepsilon_L - \left(\frac{e^2 N}{4\pi^2 \varepsilon_o m^* c^2}\right)\lambda^2 \quad (5)$$

$$\varepsilon_i = 2nk \quad (6)$$

where ε_L is the lattice dielectric constant, ε_o is the permittivity of free space, and $\frac{N}{m^*}$ is the ratio of carrier concentration to its effective mass. Fig. 11 shows the relation between ε_r versus λ^2 for the as deposited and annealed Ru-complex thin films. The ratio of carrier concentration to the effective mass, N/m^*, is calculated using equation (5) from the slope of the straight line, by extrapolating the linear part of the curve towards the shorter wavelength, the intercept with the vertical axis (at $\lambda^2 = 0$) is directly the value of ε_L. The calculated values of N/m^* *and* ε_L are listed in Table 1. It is noticed from the table that annealing increases the values of the dispersion parameters of the complex.

The spectral behaviors of ε_r and ε_i as a function of the incident photon energy, $h\nu$, for the as deposited and annealed Ru-complex thin films are shown in Fig. 12 a and 12 b. It is observed from the two figures that annealing decreases the values of ε_r but increases the values of ε_i.

The volume and surface energy loss function (VELF and SELF) can be calculated using equations (7) and (8) [39]:

$$SELF = \frac{\varepsilon_2}{(\varepsilon_1 + 1)^2 + \varepsilon_2^2} \quad (7)$$

$$VELF = \frac{\varepsilon_2}{(\varepsilon_1^2 + \varepsilon_2^2)} \quad (8)$$

Fig. 13 (a) and (b) show the VELF and SELF as a function of the incident photon energy. It is clear that the values of SELF are smaller than those of VELF for the as deposited and annealed Ru-complex thin film.

3.7.3. Absorption characteristics

Fig. 14 shows the spectral distribution of the absorption index, k. It is noticed that thermal annealing increases the values of k. The spectral behavior of k shows absorption bands at 252, 300, 370 and 500 nm which are the same found for the molecular complex in solution (Fig. 5) discussed in section 3.4. We can notice that there exists a small shift between the peaks of thin film and the complex in solution which can be attributed to the effect of solvent [40]. The optical absorption coefficient, α, as a function of energy is shown in Fig. 15. The values of the optical energy gap (E_g) can be estimated using Bardeen equation [41]:

$$\alpha\, h\nu = B(h\nu - E_g^{opt})^x, \quad (9)$$

where B is a constant related to the electrical conductivity and energy level separation, $x = 2$ or 3 for indirect allowed and forbidden transitions, respectively and $x = 1/2$ or $3/2$ for direct allowed and forbidden transitions, respectively.

The experimental data were fitted with the theoretical (Eq. (9)) for different values of x. The best fit is obtained for $x = 2$, which indicates that the transition type is indirect allowed one.

Fig. 16 shows $(\alpha h\nu)^{1/2}$ versus $h\nu$ for as deposited and annealed Ru-complex films. The values of the onset and fundamental band gaps are listed in Table 2. It is noticed that annealing decreases the value of the onset band gap but increases the value of the fundamental band gap. This change in the band gaps can be attributed to structural disorders that could happen to the thin film structure due to annealing.

4. Conclusions

The new $[Ru(bpy)_2(Hapbim)]^{2+}$ complex derived from *cis*-$[Ru(bpy)_2Cl_2].2H_2O$ and 2-aminophenylbenzimidazole (Hapbim) was prepared and characterized. The ligand binds to the Ru(II) ion in a neutral bidentate (N, N) manner through amino group and cyclic azomethine nitrogen atoms in octahedral geometry. Thin films of the synthetized complex were prepared using thermal evaporation technique. FTIR analysis proved the chemical stability of the complex under thermal evaporation technique and annealing of the thin films at 423 K. XRD analysis of the investigated Ru(II)-complex in the powder form revealed that it has polycrystalline structure with triclinic crystal system. XRD analysis of the as deposited and annealed thin films revealed that both cases have amorphous structure. The Ru(II)-complex showed excellent optical properties with small energy gap of 1.49 eV which was decreased by annealing to 1.38 eV. Annealing of the thin films increased the values of the dispersion parameters. The investigated complex possesses excellent absorption characteristics which makes it a potential material in optoelectronic applications such as solar cells and OLEDs.

Acknowledgments

We dedicate this work to the memory of Prof. Dr. H. M. Zeyada. We are also grateful to Prof. Dr. Ahmed M. El-Hendawy for providing us with the starting material *cis*-$[Ru(bpy)_2Cl_2].2H_2O$.

References

[1] E.R. Dos Santos, M.A. Mondelli, L.V. Pozzi, R.S. Corrêa, H.S. Salistre-de-Araujo, F.R. Pavan, C.Q. Leite, J. Ellena, V.R. Malta, S.P. Machado, New ruthenium (II)/phosphines/diimines complexes: promising antitumor (human breast cancer) and Mycobacterium tuberculosis fighting agents, Polyhedron 51 (2013) 292–297.
[2] B.-B. Ma, Y.-X. Peng, T. Tao, J. Geng, W. Huang, Ruthenium sensitizers with various 2-thiophenimidazo [4, 5-f][1, 10] phenanthroline based ancillary ligands and their performance for dye-sensitized solar cells, Dyes Pigments 117 (2015) 100–107.
[3] C. Dragonetti, A. Colombo, M. Magni, P. Mussini, F. Nisic, D. Roberto, R. Ugo, A. Valore, A. Valsecchi, P. Salvatori, Thiocyanate-free ruthenium (II) sensitizer with a pyrid-2-yltetrazolate ligand for dye-sensitized solar cells, Inorg. Chem. 52 (2013) 10723–10725.
[4] H. Shahroosvand, F. Nasouti, A. Sousaraei, Ruthenium (II) multi carboxylic acid complexes: chemistry and application in dye sensitized solar cells, Dalton Trans. 43 (2014) 5158–5167.
[5] F. Meyer, H. Kozlowski, J.A. McCleverty, T.J. Meyer (Eds.), Comprehensive Coordination Chemistry II: from Biology to Nanotechnology, Elsevier, Oxford, 2004.
[6] Y. Zhu, C. Gu, S. Tang, T. Fei, X. Gu, H. Wang, Z. Wang, F. Wang, D. Lu, Y. Ma, A new kind of peripheral carbazole substituted ruthenium (II) complexes for electrochemical deposition organic light-emitting diodes, J. Mater. Chem. 19 (2009) 3941–3949.
[7] A. Hagfeldt, G. Boschloo, L. Sun, L. Kloo, H. Pettersson, Dye-sensitized solar cells, Chem. Rev. 110 (2010) 6595–6663.
[8] J.N. Clifford, E. Martínez-Ferrero, A. Viterisi, E. Palomares, Sensitizer molecular structure-device efficiency relationship in dye sensitized solar cells, Chem. Soc. Rev. 40 (2011) 1635–1646.
[9] K.C. Robson, P.G. Bomben, C.P. Berlinguette, Cycloruthenated sensitizers: improving the dye-sensitized solar cell with classical inorganic chemistry principles, Dalton Trans. 41 (2012) 7814–7829.
[10] M. Montalti, A. Credi, L. Prodi, M.T. Gandolfi, Handbook of Photochemistry, CRC press, 2006.
[11] H. Ozawa, T. Sugiura, T. Kuroda, K. Nozawa, H. Arakawa, Highly efficient dye-sensitized solar cells based on a ruthenium sensitizer bearing a hexylthiophene modified terpyridine ligand, J. Mater. Chem. 4 (2016) 1762–1770.
[12] A. Colombo, C. Dragonetti, A. Valore, C. Coluccini, N. Manfredi, A. Abbotto, Thiocyanate-free ruthenium (II) 2, 2′-bipyridyl complexes for dye-sensitized solar cells, Polyhedron 82 (2014) 50–56.

[13] J.G. Vos, J.M. Kelly, Ruthenium polypyridyl chemistry; from basic research to applications and back again, Dalton Trans. (2006) 4869–4883.
[14] M. Buda, G. Kalyuzhny, A.J. Bard, Thin-film solid-state electroluminescent devices based on tris (2, 2 '-bipyridine) ruthenium (II) complexes, J. Am. Chem. Soc. 124 (2002) 6090–6098.
[15] K. Ocakoglu, S. Okur, H. Aydin, F.M. Emen, The effect of annealing temperature on the optical properties of a ruthenium complex thin film, Thin Solid Films 612 (2016) 225–230.
[16] P.A. Praveen, R. Ramesh Babu, K. Jothivenkatachalam, K. Ramamurthi, Spectral, morphological, linear and nonlinear optical properties of nanostructured benzimidazole metal complex thin films, Spectrochim. Acta Mol. Biomol. Spectrosc. 150 (2015) 280–289.
[17] P.A. Praveen, R.R. Babu, K. Ramamurthi, Role of annealing on the structural and optical properties of nanostructured diaceto bis-benzimidazole Mn(II) complex thin films, Spectrochim. Acta Mol. Biomol. Spectrosc. 173 (2017) 800–808.
[18] K.B. Manjunatha, R. Rajarao, G. Umesh, B. Ramachandra Bhat, P. Poornesh, Optical nonlinearity, limiting and switching characteristics of novel ruthenium metal-organic complex, Opt. Mater. 72 (2017) 513–517.
[19] B. Sullivan, D. Salmon, T. Meyer, Mixed phosphine 2, 2′-bipyridine complexes of ruthenium, Inorg. Chem. 17 (1978) 3334–3341.
[20] H.M. Zeyada, N.A. El-Ghamaz, M.I. Youssif, E.A. Gaml, Effect of annealing and UV irradiation on structural and optical properties of 6-(3,4 Dimethoxyphenyl)-1-methyl-3-oxo-2-phenyl-2,3-dihydro1Hpyrazolo[4,3-b]-5-carbonitrile thin films, Opt. Mater. 69 (2017) 392–400.
[21] N. Biradar, T. Goudar, Addition compounds of niobium (V) with 2-substituted benzimidazoles, J. Inorg. Nucl. Chem. 39 (1977) 358–360.
[22] J. Małecki, Half-sandwich ruthenium (II) complexes with N-and N,(N, O)-donor ligands: molecular, electronic structures, and computational study, Struct. Chem. 23 (2012) 461–472.
[23] P. Tamayo, M.A. Mendiola, J.R. Masaguer, C. Molleda, Tin (IV), titanium (IV) and vanadium (IV) chloride complexes with 2-aminobenzimidazole and 2 (2′-aminophenyl) benzimidazole, Transit. Met. Chem. 14 (1989) 283–286.
[24] S.A. Elsayed, B.J. Jean-Claude, I.S. Butler, S.I. Mostafa, Synthesis, structural characterization and anticancer activity of some new complexes of 6-amino-4-hydroxy-2-thiopyrimidine, J. Mol. Struct. 1028 (2012) 208–214.
[25] A. Kumar, A. Kumar, R.K. Gupta, R.P. Paitandi, K.B. Singh, S.K. Trigun, M.S. Hundal, D.S. Pandey, Cationic Ru (II), Rh (III) and Ir (III) complexes containing cyclic π-perimeter and 2-aminophenyl benzimidazole ligands: synthesis, molecular structure, DNA and protein binding, cytotoxicity and anticancer activity, J. Organomet. Chem. 801 (2016) 68–79.
[26] P. Amudha, P. Akilan, M. Kandaswamy, Synthesis, spectral, electrochemical and magnetic properties of new symmetrical and unsymmetrical dinuclear copper (II) complexes derived from binucleating ligands with phenol and benzimidazole donors, Polyhedron 18 (1999) 1355–1362.
[27] R. Rohini, K. Shanker, P.M. Reddy, V. Ravinder, Synthesis and antimicrobial activities of a new class of 6-arylbenzimidazo [1, 2-c] quinazolines, J. Braz. Chem. Soc. 21 (2010) 49–57.
[28] S.L. Everitt, M.B. Drew, Preparation and structural elucidation of novel cis ruthenium (II) bis (bipyridine) sulfoxide complexes, J. Chem. Soc., Dalton Trans. (1999) 3701–3709.
[29] Z. Lv, W. Zheng, Z. Chen, Z. Tang, W. Mo, G. Yin, Synergistic oxygen atom transfer by ruthenium complexes with non-redox metal ions, Dalton Trans. 45 (2016) 11369–11383.
[30] D.J. Charboneau, N.A. Piro, W.S. Kassel, T.J. Dudley, J.J. Paul, Reprint of: structural, electronic and acid/base properties of [Ru (bpy)(bpy (OH) 2) 2] 2 + (bpy = 2, 2′-bipyridine, bpy (OH) 2 = 4, 4′-dihydroxy-2, 2′-bipyridine), Polyhedron 114 (2016) 472–481.
[31] A. Ghosh, A. Mandoli, D.K. Kumar, N.S. Yadav, T. Ghosh, B. Jha, J.A. Thomas, A. Das, DNA binding and cleavage properties of a newly synthesised Ru (II)-polypyridyl complex, Dalton Trans. (2009) 9312–9321.
[32] H.A. El-Asmy, I.S. Butler, Z.S. Mouhri, B.J. Jean-Claude, M. Emmam, S.I. Mostafa, Synthesis, characterization and DNA interaction studies of new complexes containing 2-mercaptobenzothiazole and different dinitrogen or phosphorous aromatic donors, Inorg. Chim. Acta. 441 (2016) 20–33.
[33] A.A. Shabana, I.S. Butler, D.F. Gilson, B.J. Jean-Claude, Z.S. Mouhri, M.M. Mostafa, S.I. Mostafa, Synthesis, characterization, anticancer activity and DNA interaction studies of new 2-aminobenzothiazole complexes; crystal structure and DFT calculations of [Ag (Habt) 2] ClO 4, Inorg. Chim. Acta. 423 (2014) 242–255.
[34] A.M. El-Hendawy, S.Y. Alqaradawi, H.A. Al-Madfa, Ruthenium (III) mono (2, 2′-bipyridine) complexes containing O, O-donor ligands and their oxidation properties for organic compounds, Transit. Met. Chem. 25 (2000) 572–578.
[35] T. Roisnel, J. Rodriguez-Carvajal, Computer Program FULLPROF, LLB-lcsim, (May 2003).
[36] M.M. El-Nahass, M.M. Sallam, S.A. Rahman, E.M. Ibrahim, Optical, electrical conduction and dielectric properties of TlGaSe2 layered single crystal, Solid State Sci. 8 (2006) 488–499.
[37] H.M. Zeyada, N.A. El-Ghamaz, E.A. Gaml, Effect of substitution group variation on the optical functions of -5-sulfono-7-(4-x phenyl azo)-8-hydroxy quinoline thin films, Curr. Appl. Phys. 13 (2013) 1960–1966.
[38] S.H. Wemple, M. DiDomenico, Behavior of the electronic dielectric constant in covalent and ionic materials, Phys. Rev. B 3 (1971) 1338–1351.
[39] M.M. El-Nahass, Z. El-Gohary, H.S. Soliman, Structural and optical studies of thermally evaporated CoPc thin films, Optic Laser. Technol. 35 (2003) 523–531.
[40] J. Luo, C. Yang, J. Zheng, J. Ma, L. Liang, M. Lu, Synthesis and photophysics properties of novel bipolar copolymers containing quinoline aluminum moieties and carbazole segments, Eur. Polym. J. 47 (2011) 385–393.
[41] J. Bardeen, F. Blatt, L. Hall, Photoconductivity Conference vol. 195623, Wiley, New York, 1956, p. 146.